Axial Crushing of Uni-Sectional Bi-Tubular Inner Tubes with Multiple Outer Cross-Sections

Abstract

Increase of energy absorption along with smooth load displacement curve, reduced peak force and high mean crushing force is the key in the modern dynamic design of structures. In this regard, a new metallic tubular configuration consisting of uni-sectional bi-tubular inner tubes, with outer tubes of multiple varied cross-sections is proposed and crushed under axial dynamic loading. A number of configurations are proposed ranging from simple to complex polygonal sections defined in three groups. Deformation modes and energy absorption characteristics such as peak crushing force, mean crushing force, and specific energy absorption are determined and discussed for each configuration. The proposed arrangement shows a stable crushing and higher values of crush force efficiency. In order to select the most suitable configuration, on the basis of maximum specific energy absorption, peak crushing force and minimum peak force, a robust decision making method known as Complex Proportional Assessment (COPRAS) is implemented. The optimal configuration in each group is determined on the basis of higher values of specific energy absorption, crush force efficiency and a lower value of peak crushing force, using the chosen weighting factors in COPRAS implementation. Finally, the configuration with inner and outer hexagonal tubes is found to be the best possible design concept among the top members of each group, with peak crushing force, mean crushing force and crush force efficiency values of 69.8 KN, 7.3 KJ and 0.75, respectively.

Muhammad Kamran [a, *]
Pu Xue [a]
Naveed Ahmed [a]
M S Zahran [a]
A A G Hanif [b]

[a] School of Aeronautics, Northwestern Polytechnical University, Xi'an, 710072, PR China. kamranm470@yahoo.com
p.xue@nwpu.edu.cn
engineer_naveed@yahoo.com
mz_mohamedzahran43@yahoo.com
[b] CESAT, Islamabad, Pakistan.
Ahmed.abdul.ghaffar@gmail.com

* Corresponding author

http://dx.doi.org/10.1590/1679-78254175

1 INTRODUCTION

The improvement of safety and crashworthiness features of aero or automobile systems are becoming more challenging with the advancements of transportation and aerospace engineering to protect

the humans and vulnerable equipment. The metallic thin-walled structures have proved to be a comparable choice under dynamic crushing when these demands are to be accomplished with optimal weight feature and low cost. Impact energy is absorbed by such systems in multiple mechanisms such as fracture, splitting, bending, tension, shear and plastic deformation (Jones, 2012). Metallic tubes are one such choice which show multiple deformation modes under axial crushing with unique features such as locally deformed axisymmetric or concertina mode, diamond mode, mixed mode or globally deformed Euler buckling mode depending on the geometry, material parameters and boundary conditions (Zahran et al., 2016a; Karagiozova and Alves, 2004).

Thin walled metallic tubes have been a research focus since 1960 when Alexander (1960) proposed an excellent theoretical model to access average crushing force for axisymmetric fold pattern on the basis of experimental investigations. Theoretical solutions to predict the non-symmetric or diamond deformations were provided by Wierzbicki and Abramowicz (1983). Since then, crushing of metallic tubes has always been a hot topic of research. A series of axial crushing tests on steel and aluminium tubes along with correction factor for the effective crushing distance to modify the theoretical predictions of Alexander and Wierzbicki was proposed by Abramowicz and Jones (1986). Crashworthiness improvement has been carried out by a number of researchers employing multiple cross-sectional features such as circular tubes (Aljawi and Alghamdi, 2000; Karagiozova et al., 2000), square tubes (Langseth et al., 1996; 1999), frusta (Aljawi and Alghamdi, 2000; Alghamdi et al., 2002; Hosseini et al., 2006), conical (Hui and Xiong, 2016), stepped tubes with external stiffeners (Zahran et al., 2016b), circular tubes with curvy stiffeners (Ahmed et al., 2017) and multi-corner columns (Abramowicz and Weirzbicki, 1989). Due to the better capability of Specific Energy Absorption (SEA), mutli-cell tubes gained a particular interest. Using a Simplified Super Folding Element (SSFE) theory, Chen and Weirzbicki (2001) investigated the behavior of single-cell, double-cell and triple-cell tubes under quasi-static axial crushing with the conclusion that the tripled and double cell columns were more efficient than single cell columns. Tang et al., (2013) revealed that multi-cell circular tubes are superior to square multi-cell tubes and the wall thickness, the number of cells along the radial and circumferential direction has a distinct effect on the energy absorption. Xie et al., (2017) derived a theoretical expression for the mean crushing force and SEA ratios of five different multi-cell square tubes were derived by applying the SSFE theory. He showed that the sectional form exerted a greater influence on the crushing force and energy absorption. Yafeng et al., (2017) studied an octagonal multi-cell tube with functionally graded thickness (FGT) under multiple loading angles and showed that thickness gradient exponent and thickness range have significant effect on its crashworthiness by employing the parametric study on FGT tubes. The FGT tubes were then optimized to find out the guidelines for the design of multi-cell tube with functionally graded thickness under multiple loading angles. The lateral crushing behavior of multi-cell triangular tubes is experimentally investigated and using the simplified super folding element (ISSFE) theory, theoretical models are proposed to predict average crushing force in each stage (TrongNhan Tran, 2017).

Multi-tubes configurations especially bi-tubular and step tubes were studied for crushing responses to control the energy absorption in a more refined way. Tang et al., (2013) studied the bi-tubular tubes and reported that the double layered cylindrical multi-cell column was excellent in energy absorption with appropriate peak force. A quasi-static axial compression of bi-tubular square

tubes showed that bi-tubular tubes with shorter inner tube can absorb more energy than single outer tube (Kashani et al., 2013). The concentric arrangement of tubes with filling of foam can increase the energy absorption, discussed by Manmohan Dass Gohel (2015) in the study of single, bi-tubular and tri-tubular cylindrical and square tubes under axial compression. A very recent study with bi-cross-sectional bi-tubular tubes made of steel showed that the hexagonal inner tube has more energy absorption capability than the other bi-tube combinations and the single cylinder (Vinayagar and Kumar, 2017). Yamashita et al. (2003) studied the tube with various regular polygonal cross-sections for their crashworthiness characteristics and found that the mean crushing force increases with increasing the number of the cross-section corners. Foam filling in bi-tubular tubes considerably improved the energy absorption, particularly in bi-tubular configurations (Seitzberger et al., 2000).

To improve the energy absorption capability of tubes, optimization techniques have been used by the researchers such as combined multi- criteria design optimization (MDO) technique (Zarei and Kroger, 2008), integrated particle swarm optimization (PSO) (Sun et al., 2010), genetic algorithm (Zhang et al., 2012) and complex proportional assessment (COPRAS) (Gang et al., 2014). The energy comparison of foam filled single and bi tubular polygonal tubes with different cross-sections using finite element method (FEM) and Element Free Galerkin method (EFGM) for modeling the tubes for their interaction associated with large deformation, failure and damage was employed by Gang et al., (2014) and using COPRAS, a comparison was drawn and it was concluded that the circular foam filled bi-tubular column has outstanding energy absorption. COPRAS and Kriging modeling technique along with multi objective particle optimization (MOPSO) algorithm was employed by Qiu et al., (2015) to determine the optimized cross sectional configuration from multi-cell hexagonal cross-sectional columns with enhanced crashworthiness characteristics. COPRAS showed the multi-cell members with inner tube and scale number of 0.5, and the column with circular cross-section as the better energy absorbing devices when a new design of multi-cell devices is evaluated for the crashworthiness capability of single and multi-cell members made up of two straight columns with the same shape of cross-section connected together by several ribs, proposed by Pirmohammad and Marzdashti (2016). The COPRAS is employed to rank thin-walled members with multiple polygonal shapes, crushed under axial loading, using specific energy absorption, peak crushing force and crash force efficiency as decision criterion. The multi-cell S-rail with decagonal cross-section was found to be the optimal which was further optimized using parametric study (Marzdashti et al., 2016). The COPRAS is also employed in this study to find out the best configuration among the proposed configuration in terms of energy absorption characteristics.

Although multiple configurations to improve the crashworthiness parameters have been studied under axial crushing; however multi-tubes with uni-cross-section placed inside varying cross-section to find out an ideal energy absorber is rarely studied. In this study, novel configurations of metallic tubes with bi-tubes having the same cross-section are placed inside an outer circular and varying cross-sectional tube are defined and crushed for axial loading. The finite element package ABAQUS® Explicit Dynamics is used to perform a series of numerical studies with the objective to find out the best possible configuration employing the robust decision-making method COPRAS in terms of specific energy absorption, maximum crushing force and minimum peak force. The defor-

mation modes and force-displacement curves for different configurations are also discussed to see the effect of proposed geometry of inner tubes.

2 PROPOSED STRUCTURAL CONFIGURATIONS

A set of uni-sectional inner bi-tubes configurations, broadly categorized in three groups named as Group 'A', 'B' and 'C', is proposed as shown in Figure 1. Group 'A' and 'B' have a similar outer circular tube of length L=200mm, and diameter D=80mm but different inner tubes arrangement. The Group 'A' has two inner same cross-sectional tubes placed in a way that if one is placed in first quadrant of the outer circular tube, the other is placed in the third quadrant while Group 'B' has two inner same shaped polygonal tubes placed one inside the other, both then put inside a bigger outer cylindrical tube. The Group 'C' has the same cross-section of the outer and the inner tubes; however the unique feature of uni-sectional inner bi-tubes placement is maintained on the rules, defined for Group A. The thicknesses of all the tubes are kept constant with a value of 1.5mm while all other geometry details are shown in Figure 1(a)-1(c) for each defined group. The configurations in a group are sub-categorized by assigning a Group ID followed by the ascending numerical number of configuration.
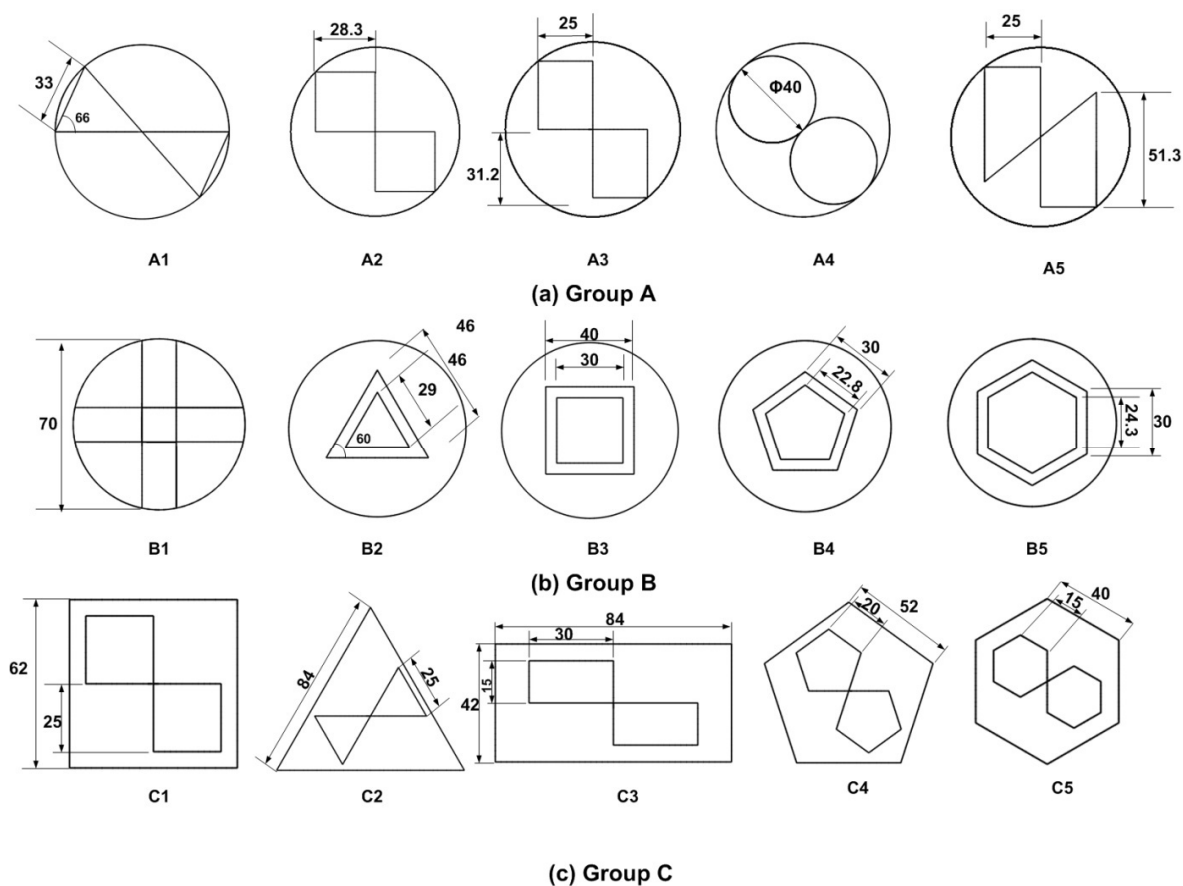

Figure 1: Proposed structural configurations (a) Group A (b) Group B(c) Group C.

All of the tubes are made of AA 6060 T4 material whose properties are tabulated in Table 1 and stress-strain curve is shown in Figure 2 (Tang et al., 2013).

Parameter	Value
Young's Modulus (GPa)	68.21
Yield Strength (MPa)	80
Ultimate Strength (MPa)	173
Ultimate Elongation (%)	17.4
Poisson's Ratio	0.3

Table 1: AA 6060 T4 material properties.
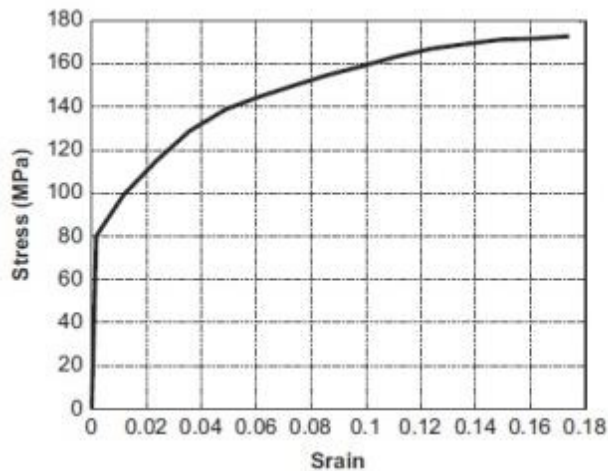
Figure 2: Stress-strain curve for AA 6060 T4 (Tang et al., 2013).

3 ANALYTICAL FORMULATION

3.1 Crashworthiness Indicators

Energy absorption parameters for a tube structure are evaluated from the force-displacement curves. The Peak Crushing Force (PCF) is defined as the first peak load in the force-displacement curve while the Mean Crushing Force (MCF) is calculated over a 70% of the tube length as it gets crushed.

MCF can be calculated as:

$$MCF = \frac{1}{(b-a)} \int_a^b F d\delta \tag{1}$$

where a is start point of crushing, b is the selected end point of crushing; in this case it is 70% of the length of the tube, F is the crushing force and δ is the crushing displacement.

Crush Force Efficiency (CFE) is defined as the ratio of the mean crushing force to the peak crushing force as shown in Equation 2:

$$CFE = {MCF}/{PCF} \tag{2}$$

Energy Absorption (EA) is the amount of energy dissipated during crushing process of the structure and can be calculated from the area under the force-displacement curve from a to b:

$$EA = \int_{a}^{b} F d\delta \tag{3}$$

Specific Energy Absorption (SEA) is the ratio of dissipated energy to the total mass (m) of the structure.

It is the ratio of absorbed energy to the total mass (m) of the structure. It is used to compare the performance of the energy absorbers and can be calculated as:

$$SEA = {EA}/{m} \tag{4}$$

3.2 Complex Proportional Assessment (COPRAS)

To choose the best design concept among different design alternatives, a multi-criteria decision making methods is needed. For this purpose, a decision making method known as Complex Proportional Assessment (COPRAS) method was employed. Zavadskas, Kaklauskas and Sarka, first developed this method in 1994. This method can be applied in the field of Economics, Construction, Manufacturing and design engineering. This decision making method considers different alternatives and compares them with respect to multiple conflicting criteria by assigning different weights to each selection criteria. Finally, a complete ranking of different design concepts can be made by following the steps mention below;

Step 1: Make the initial decision making matrix as below;

$$X = \left[x_{ij}\right]_{mn} = \begin{bmatrix} x_{11} & x_{12} & & x_{1n} \\ x_{21} & x_{22} & & x_{2n} \\ ... & ... & ... & ... \\ x_{m1} & x_{m2} & & x_{mn} \end{bmatrix} \tag{5}$$

where x_{ij} denotes the performance value of ith alternative against the jth design criteria and m and n shows the numbers of design alternatives and design criterions.

Step 2: Normalize the decision matrix X, as Normalized decision matrix R is required to obtain dimensionless values of different conflicting criteria so that they can be compared.

$$R = \left[r_{ij}\right]_{mn} = \frac{x_{ij}}{\sum_{i=1}^{m} x_{ij}} \tag{6}$$

Step 3: Determine the weighted normalize decision matrix D as below:

$$R = \left[y_{ij}\right] = r_{ij} \times w_{j} \tag{7}$$

where r_{ij} is the normalized performance value of ith alternative against j^{th} criteria and w_j is the weightage of jth criteria. The sum of the normalized weight for each criteria is always equal to the weight of that mentioned criteria and is given below in Equation 8,

$$\sum_{i=1}^{m} y_{ij} = w_j \tag{8}$$

For computing the individual weightage of each criteria w_j, the following procedure can be followed (Tarlochan et al., 2013; Na Qiu et al., 2015):

i. Compare two criteria at a time. The total number of comparison sets are equal to N = n(n-1)/2, where n is the number of selection criteria.

ii. For scoring two criterions at a time, the criterion which is most important should be given a score of 3 whilst the least important criteria should be given a score of 1. If both criteria are of equal importance then give them a score of 2 each. This procedure should be repeated for all the criteria.

iii. The total score obtains against each criterion is determined as:

$$\sum_{i=1}^{m} N_{ij} = W_j \tag{9}$$

iv. The relative weighting factor w_j for each selection criteria is determined by dividing the total score for each selection criteria W_j by the global total score as shown in Table 3.

Step 4: Summation of beneficial and non-beneficial attributes:

Normalized decision matrix contains both beneficial and non-beneficial attributes. On one hand a high value of beneficial attribute is better while on the other hand a low value of non-beneficial attribute is preferable. For example, a low value of PCF (non-beneficial attribute) is preferable for good energy absorber while a high value of SEA (beneficial attribute) is better for a best energy absorber. Sum of beneficial and non-beneficial attributes can be determined as follows:

$$S_{+i} = \Sigma_{j=1}^{n} y_{+ij} \tag{10}$$

$$S_{-i} = \Sigma_{j=1}^{n} y_{-ij} \tag{11}$$

where the y_{+ij} and y_{-ij} are the weighted normalized values of beneficial and non-beneficial attributes. The sum of Equations 10 and 11 is always equal to 1.

Step 5: Determination of relative significance or Priority (Q)

The priority or relative significance of design alternatives are calculated as below:

$$Q_i = S_{+i} + \frac{S_{-\min} \Sigma_{i=1}^{m} S_{-i}}{S_{-i} \Sigma_{i=1}^{m} (\frac{S_{-\min}}{S_{-i}})} \tag{12}$$

where S_{-min} is the minimum value of S_{-i}.

The value of Q_i shows the degree of satisfaction attain by the concept under consideration.

Step 6: Determine the quantitative Utility (U):

The value of utility U_i completely ranked the different alternative and can be calculated as follow:

$$U_i = (\frac{Q_i}{Q_{\max}}) \times 100\% \tag{13}$$

where Q_{max} value indicates the maximum value of the relative significance. The greater the value of U_i the better is the design alternative. Design alternative with utility value of 100% is considered to be the best choice.

4 FINITE ELEMENT MODELING

Dynamic axial crushing of the proposed configurations is performed in ABAQUS explicit dynamics, a commercial FE package. The structural configurations in FE are composed of two rigid plates and a tube which is sandwiched between the two plates. The top rigid plate is allowed to move in the axial direction with a constant velocity of 10m/s while the opposite plate is restrained in all degrees of motion. The shell S4R element which is a 4-node doubly curved thick or thin shell element, is used for tube configuration meshing while the rigid plates are meshed by using discrete rigid element. Feasible mesh size of 2 mm is found to be optimal after a series of convergence studies. A general explicit contact with frictional tangential behaviour using a frictional coefficient of 0.2 and hard contact is defined for the interaction. Tube and lower plates are tied together and to avoid the inter-penetration, a self-contact is also defined for all of the elements of the configuration.

4.1 Validation of FE Model

Two experimental studies (Xiong Zhang et al., 2015; Zhang and Zhang, 2014) are selected to verify the numerical modeling adopted in the current study. The selected tubes are circular in shapes which are experimentally crushed in order to find out the crushing and energy absorption responses with material properties which are quite close to the current study. The validation is performed by keeping the structural geometry, material properties and the boundary conditions exactly the same as those in the mentioned studies. The deformation modes and force-displacement curve of the present numerical study are compared with Xiong et al., (2015) as shown in Figure 3(a) and 3(b), respectively. The concertina modes and fold formation instances are quite similar to the experimental results. The mean crushing force from the numerical study is found as 36.5KN while the experimental value was 39.2KN. Figures 3(c) and 3(d) show the comparison of experimental results of deformation and force-displacement curves with the present numerical approach with very small differences; also observed by Zhang and Zhang while performing numerical simulations due to welding attachments in experiments. The results of Figure 3 indicate that the current methodology may be used for the numerical simulation as the validation process is validated for mentioned experiments.
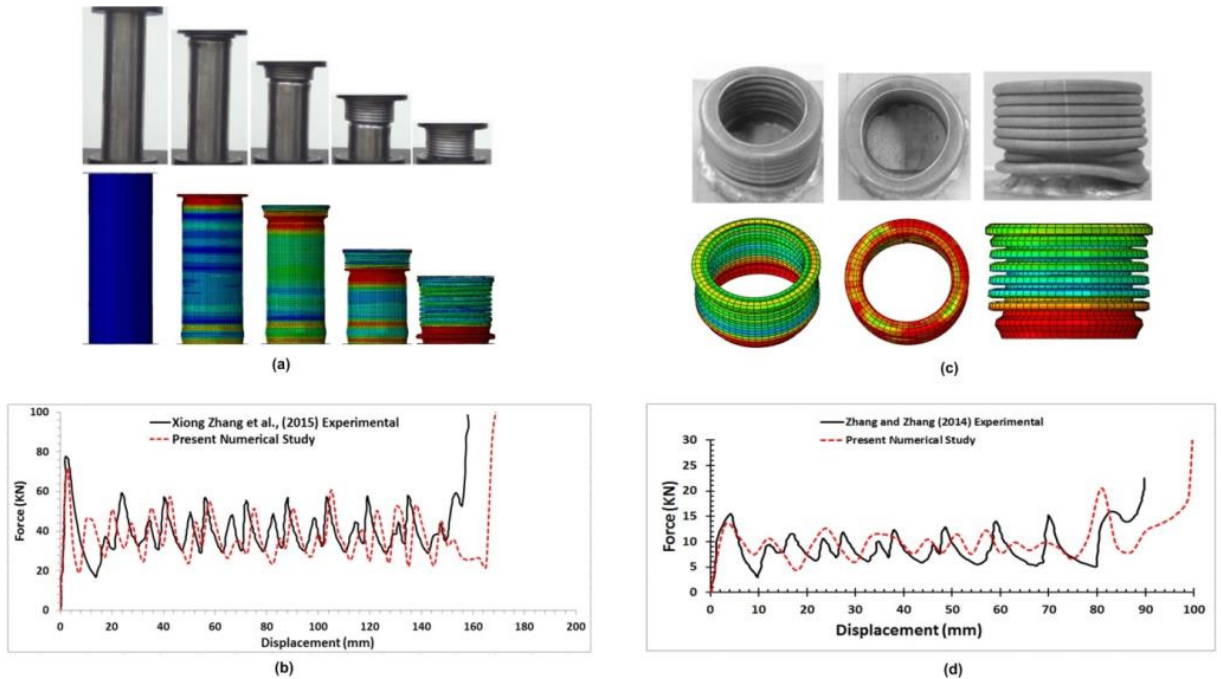
Figure 3: FE Model validation for single tube (a) Deformation plots (b) Force displacement curve [Xiong Zhang et al., vs. Current study] (c) Deformation plots (d) Force displacement curve [Zhang and Zhang et al., vs. Current study]

5   RESULTS AND DISCUSSION

5.1 Deformation Modes

The circular thin walled tubes show predominantly concertina modes under dynamic crushing when crushed without any addition of stiffeners or attachments. The deformation modes change considerably when they are crushed with some addition or stiffened panels. Deformation modes of the proposed configurations are shown in Figures 4(a)-4(c) for the Groups 'A', 'B' and 'C', respectively. Except the outer circular tubes of configurations B2-B5 of Group 'B' which show the concertina modes of deformation, all other configurations and the inner polygonal tubes of the earlier mentioned configurations of Group 'B' show the diamond modes of deformation. The number of crushing folds is different in different proposed configurations whose details are compiled in Table 2. In the initial stages of crushing, the first fold always formed at the impacted end of the tube structures with a radially outward buckle. The first local fold corresponds to the initial maximum load, which is the maximum load during the crushing process, required to overcome the friction force between the tube surface and the rigid plate. This load compels the edge for radially inward movement.

Group 'A' configuration predominantly shows diamond modes of deformation with varying number of folds in specific configurations as the tubes structures are fully compressed as shown in Figure 4(a). The first fold in all of the configurations of this group is concertina whom formation experiences elastic compression. In the later stage, plastic buckling may develop and shape of the next fold is developed from the first fold. The configuration A1 shows only one concertina mode of

deformation, converted into diamond pattern for the next four folds while all other configurations of this group show initial two concertina folds followed by three diamond modes.
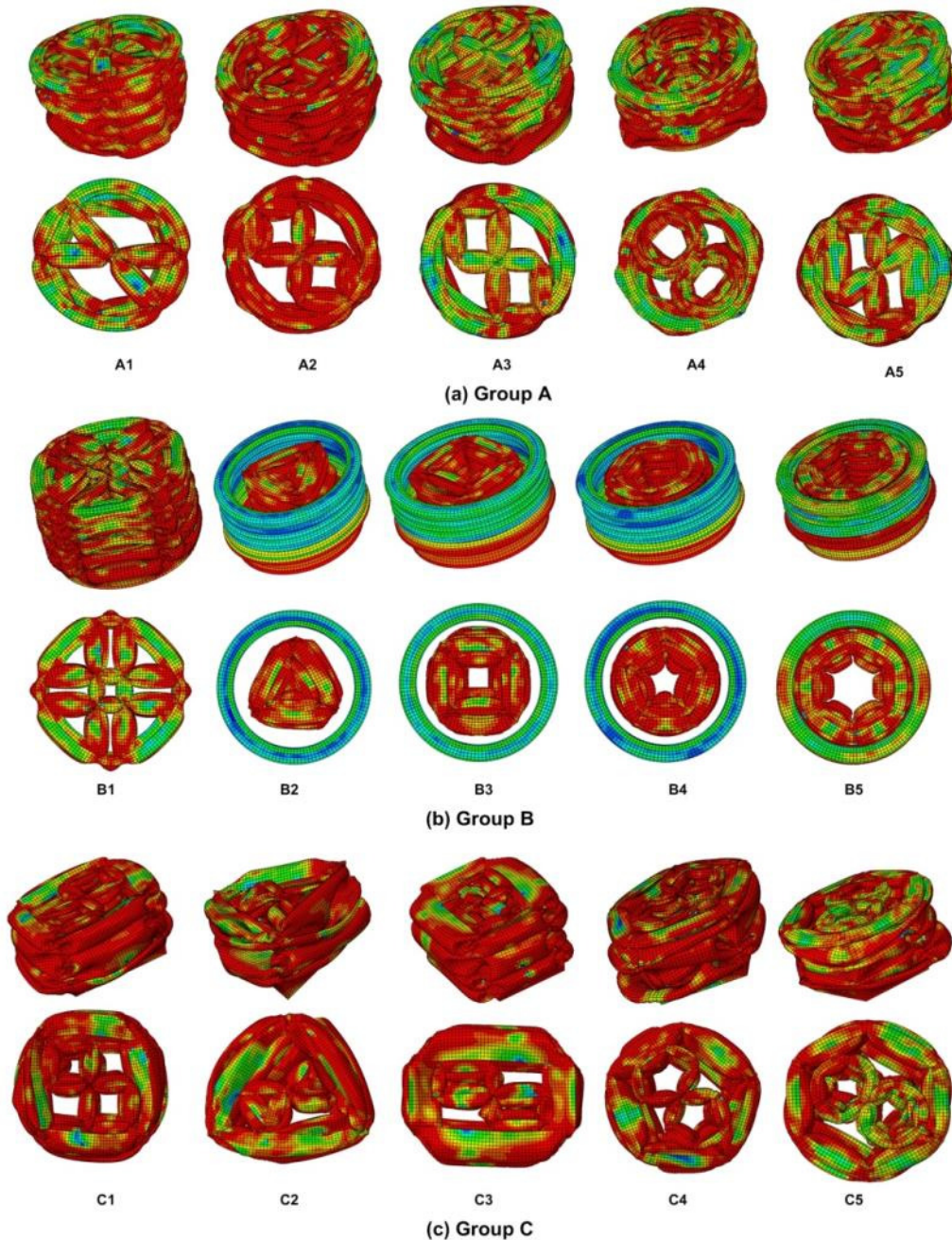

Figure 4: Deformation plots (a) Group A (b) Group B (c) Group C.

Group 'B' configurations are shown in Figure 4(b) from which it is cleared that when no connection is developed between the outer and inner tubes, the outer tube shows concertina modes of deformation as can be seen for configurations B2-B5. The B1 configuration shows five diamond

modes after the initial concertina mode while all other configurations show different deformation modes for outer circular tube and inner polygonal tubes. The outer circular tube shows eight concertina modes of deformation in B2-B5 case each while the inner tubes show five and three diamond modes for B2 and B3 respectively. As the number of walls increases in B4 and B5 case, the inner tubes collapses with complex modes, initially starting from impacted end and then after initial two folds, the other end starts forming folds which ends on a sudden collapse.

Group 'C' configurations show diamond modes in most of the configurations as shown in Figure 4(c). The square tube configuration with 2 inner square tubes shows a concertina mode of deformation near the fixed face and then diamond modes starting to happen from the impacted end leading to three diamond modes ultimately. Configuration C2 and C3 shows four diamond modes each starting from the impacted face. The configuration C4 and C5 starts collapsing with a concertina mode, later converting into diamond modes. The C4 shows three diamond modes while C5 shows four diamond modes of deformations at the full collapse.

Configuration	Mass (g)	Modes of Deformation
A1	386	1 Concertina, 4 Diamonds
A2	387	2 Concertina, 3 Diamonds
A3	386	2 Concertina, 3 Diamonds
A4	407	2 Concertina, 2 Diamonds
A5	430	2 Concertina, 3 Diamonds
B1	458	1 Concertina, 5 Diamond
B2	386	8 Concertina (Outer), 5 Diamond (Inner)
B3	430	8 Concertina (Outer), 1 Concertina, 3 Diamond (Inner)
B4	417	8 Concertina (Outer), 1 Concertina, 4 Mix [2 top then 2 Bottom] (Inner)
B5	467	8 Concertina (Outer), 1 Concertina, 4 Mix [2 top then 2 Bottom] (Inner)
C1	363	1 concertina starting near bottom end, 3 Diamond (Starting from Top Face)
C2	326	4 diamond (Top Face)
C3	350	4 diamond (Top Face)
C4	373	1 Concertina, 3 Diamond
C5	340	1 Concertina, 4 Diamond

Table 2: Folds in the proposed configurations.

5.2 Energy Absorption Responses

5.2.1 Force Displacement Curves

Force-displacement curves for all of the proposed configurations are shown in Figures 5 to 7. Without actually using the triggers in the configurations which increase the crush force efficiency but reduce the mean crushing force and energy absorption, the proposed system of configurations shows remarkably smoothed crushing process of the tubes. After the first peak load drop, the force value

shows very less variation about the mean value up to the end of the crushing process. During the formation of the first peak, the structure is free from deformations while the next peaks are influenced by the already built folds; hence the deformation in these configurations is guiding the peaks showing the effectiveness of the proposed arrangements of uni-section bi-tube arrangement.

Group 'A' configurations show quite smooth force-displacement curves with an almost constant initial peak force as the number of wall of polygons of the inner bi-tubes increased from three to four in configurations A1 to A3. The force-displacement curve is influenced by the section geometry as the peak force is changing from A3 to A5 configurations showing that the thickness, diameter or length may affect the energy absorption capability of the structure as shown in Figure 5. The circular configuration A4 shows relatively high force deviation during the fold formations with less number of folds as mentioned earlier in Table 2. The configuration A5 shows the highest peak force with earlier densification.
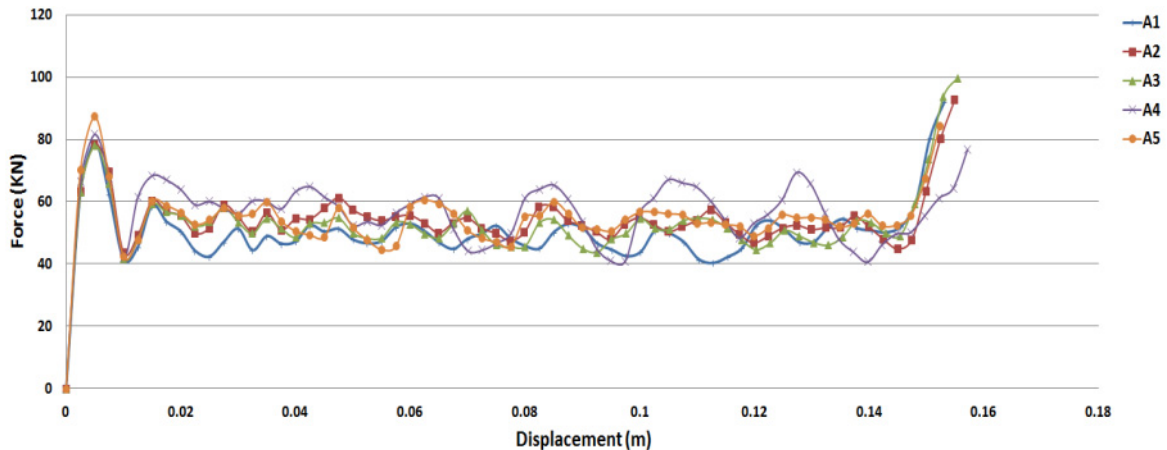

Figure 5: Force-displacement curves for Group A.

The diamond mode and mix mode absorb slightly less energy than the concertina mode; hence undesirable but the cross-section and initial collapse guide the deformation modes and control on deformation process is a complex phenomenon. The energy absorption mainly depends on the amount of plastic deformation which takes place under axial loading and concertina modes provide better plastic deformation, hence desirable. Group 'B' outer tubes show the concertina modes but the inner tube configurations shows diamond or complex modes of deformation. The configuration B2 shows different behaviour with high peak force and bigger area under the curve because of the direct connection between the outer tube and bi-walled stiffeners as shown in Figure 6. The crushing process shows a consistent behaviour of crushing with diamond modes of deformation. All other configurations show similar response for inner and outer tubes; hence not much variation is observed in the curves except the peak force increase with increasing number of walls of the inner polygons and relatively higher forces along the crushing process. B5 shows the highest peak force while B2 shows the opposite with less force along the crushing process as clear from the Figure 6.
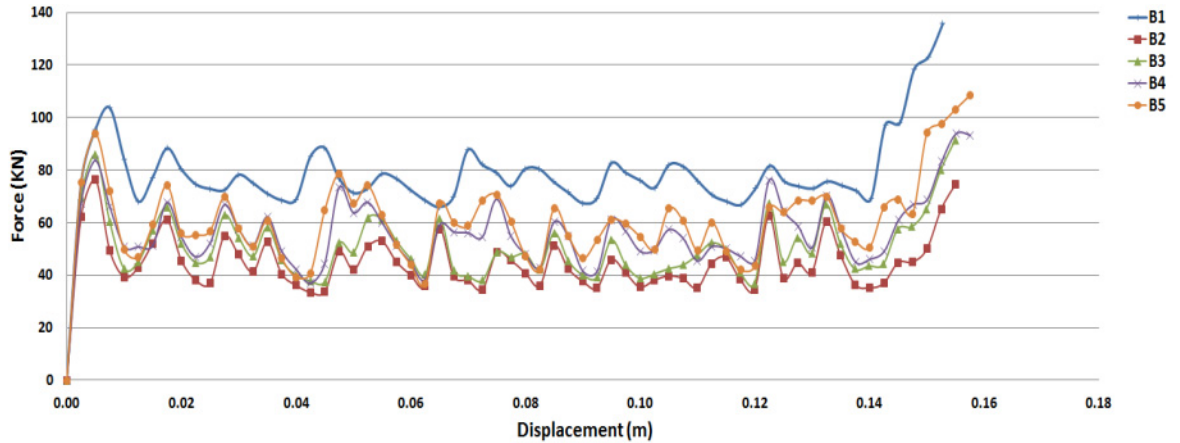
Figure 6: Force-displacement curves for Group B.

The force-displacement curves for the Group 'C' configurations are shown in Figure 7. The variation of outer tube from circular to polygonal shape shows a considerable decrease in PCF values with relatively stable crushing in configurations such as C4 and C5. The stroke length before densification is shortest in C2 and longest in C4 and C5 configurations. Configurations C4 and C5 maintains the crushing forces very close to the initial peak load suggesting a better SEA and EA values.
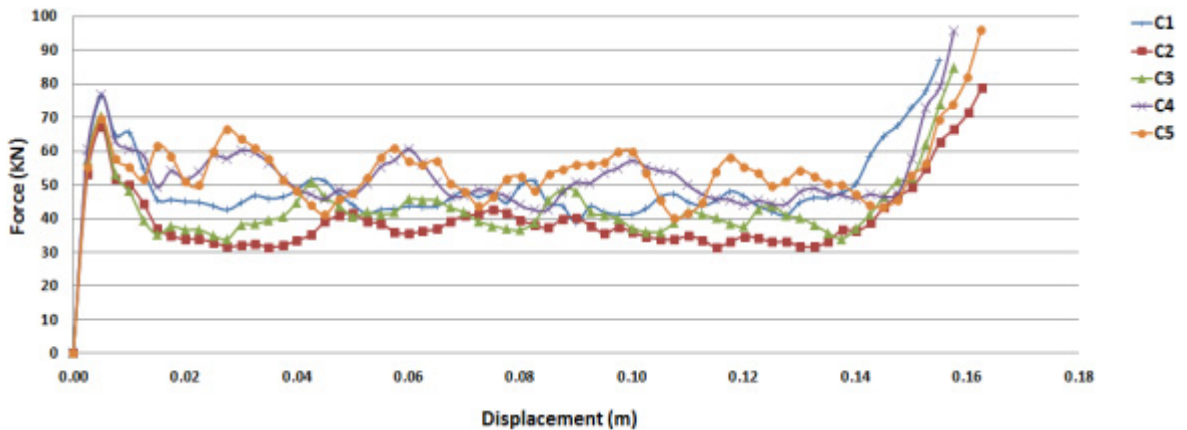
Figure 7: Force-displacement curves for Group 3.

5.2.2 Energy Absorption Indicators

Energy absorption characteristics are determined from force displacement curves of each configuration using Equations 1 to 4 which are shown in Figures 8 and 9. The values of PCF, MCF, EA and SEA for all of the proposed configurations are compared in Figures 8 while CFE in Figure 9. The initial three configuration of Group 'A' shows a very consistent behaviour in terms of EA, SEA, PCF and MCF; however the configuration A2 shows the highest SEA, MCF and EA with less PCF among the three configurations. The configuration A4 shows 5.8% , 4.14%, 10.1% higher MCF, SEA and EA, respectively in comparison to A2 configuration at the cost of 4% higher PCF as depicted in

Figure 8(a). Configuration A5 shows a PCF of 87.4KN with comparative MCF of 56.4KN; however the EA and SEA were less than A4 configuration. Among Group B, the B1 configuration shows MCF of 74.9KN but with increased PCF of 103.7KN. The SEA is the highest among the group with a value of 23kJ/kg. Other configurations show lower PCF values with less energy absorption indicators. B4 configuration with a pentagon tube system shows MCF of 53.9KN and SEA of 18.1kJ/kg. B5 configuration results are also very much similar in nature with a slight increase in values including PCF as shown in Figure 8(b).
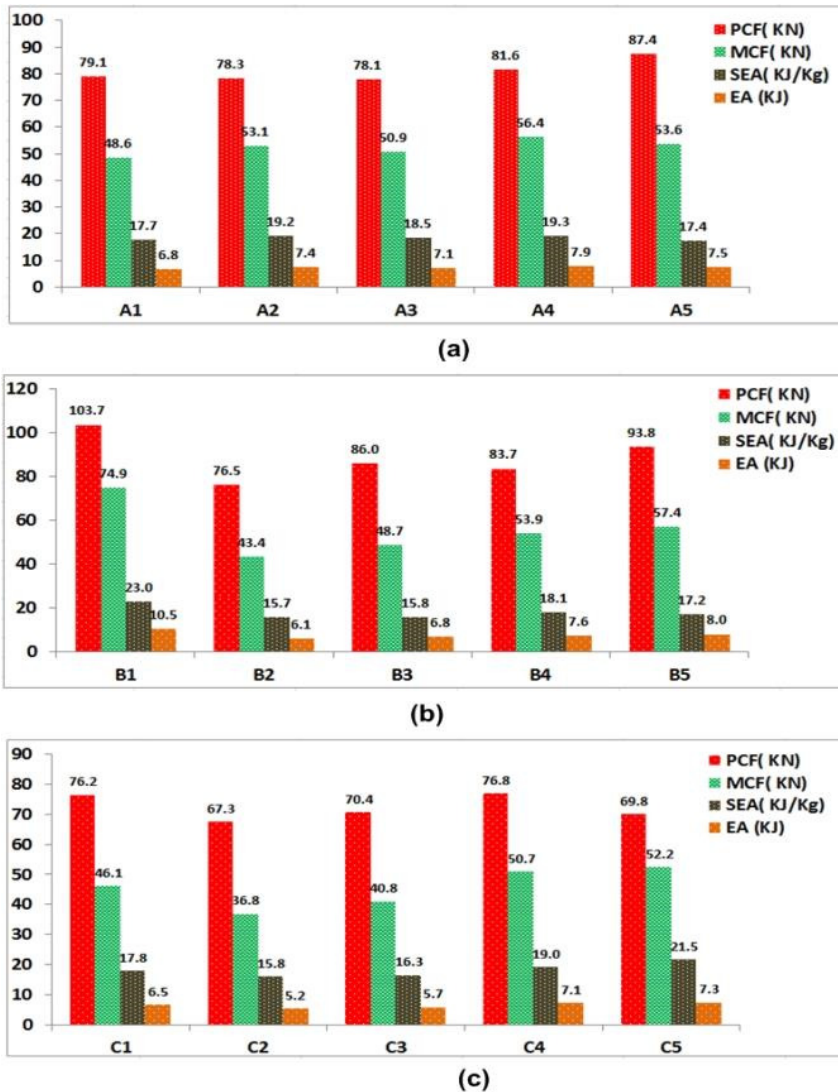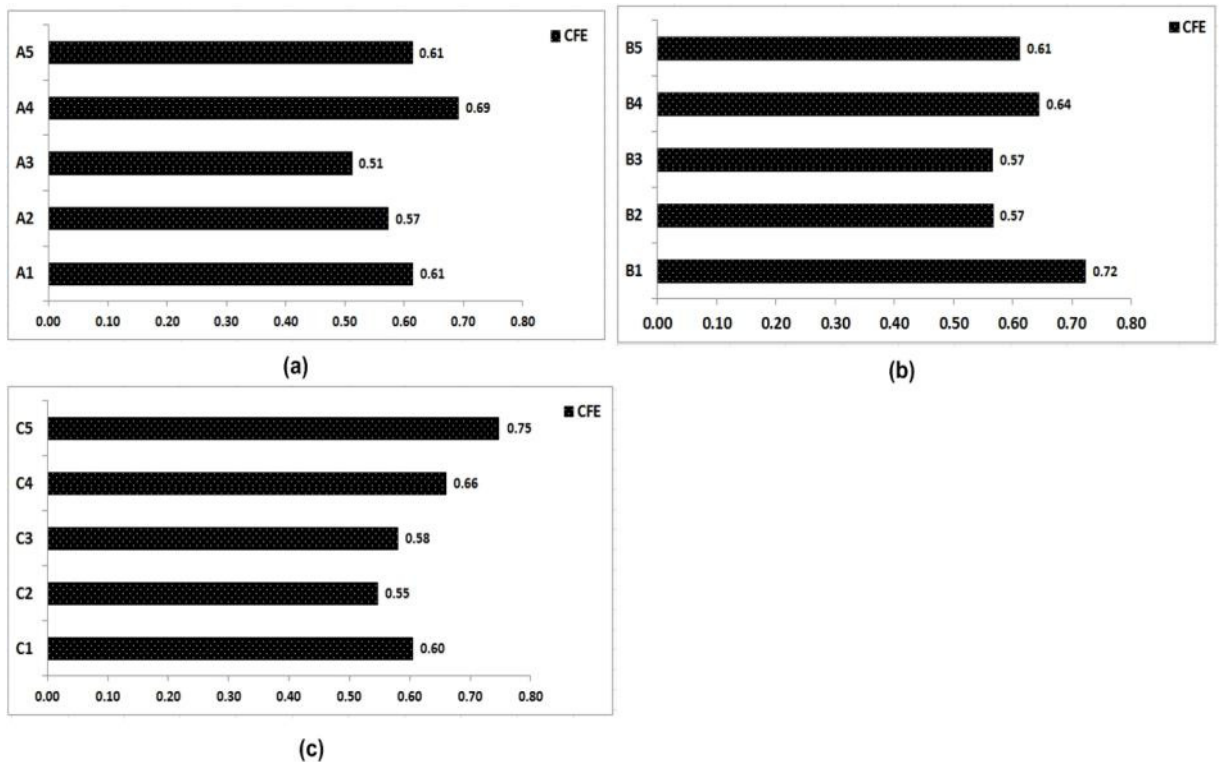

Figure 8: A comparison of energy absorption characteristics of the proposed
configurations (a) Group A (b) Group B (c) Group C.

Group 'C' configurations shows relatively low PCF values in comparison to Group 'A' and 'B' with the second best SEA in C5 after the B1 configuration. The PCF is 32.7% lower in C5 as com-

pared to B5, with only 6.5% less value of SEA. Configuration C4 shows the highest PCF in the group with a value of 76.8KN with SEA value of 19kJ/kg, second best one in the group. The lowest performance was shown by configuration C2, showing the least effective configuration though the number of walls is higher in comparison to C4 and C5 configurations.

An ideal energy absorber's CFE must approach to 100% as it is an indicator of the performance consistency of the structure. Figure 9(a)-9(c) shows the CFE values for Group 'A', 'B' and 'C', respectively. Configuration A4, B1 and C5 shows the highest values in respective group with 69%, 72% and 75% values respectively. The second and third configuration in each group shows lower values while the fourth and fifth configurations shows the highest with exception of B1 in Group 2.

Figure 9: A comparison of CFE for proposed configurations (a) Group A (b) Group B (c) Group C.

5.3 Selection of Best Energy Absorber

To select the best energy absorbing configuration, amongst all of the three groups with five configurations in each, a robust decision making method COPRAS is implemented in this study as explained in Analytical Formulation Section. For this purpose three different conflicting criteria namely SEA, PCF and CFE are considered to find the optimal design alternative. A good energy absorber needs to have a high value of SEA and CFE; it is also desirable to have a low value of PCF which is required for the safety of occupants. To this purpose, individual weightage of each

criterion is calculated as defined in step 3 of COPRAS analytical formulation section and tabulated in Table 3 by giving a score of 2 to SEA and PCF while a score of 1 to CFE.

Selection Criteria	Number of performance sets, N = n(n-1)/2 = 3(3-1)/2 = 3			W_j	w_j
	1	2	3		
PCF (KN)	2	3	-	5	5/12 = 0.417
SEA (KJ/Kg)	2	-	3	5	5/12 = 0.417
CFE	-	1	1	2	2/12 = 0.167
	Global = 12				

Table 3: Individual weightage for each selection criteria.

Among these three selecting criteria, SEA and CFE are beneficial attributes and requires high values while PCF is a non-beneficial attribute and a low value is desirable. In the first step of COPRAS method, a decision making matrix is generated for each group, using Equation 5 and the values for each group are shown in Tables 4(a), 5(a) and 6(a) for Group 'A', 'B' and 'C', respectively. In the next step, normalized decision making matrix is developed using Equation 6 to make the comparison of different conflicting criteria and values for Group 'A', 'B' and 'C' are listed in Tables 4(b), 5(b) and 6(b), respectively. In the third step, weighted normalized decision making matrix is generated for each group using Equation 7 and the results are shown in Tables 4(c), 5(c) and 6(c) for the three groups. As already mentioned weighted normalized decision making matrix contain both beneficial and non-beneficial attributes; summation of weighted normalized beneficial and non-beneficial attributes are calculated for each group by using Equations 10 and 11 and can be seen in Tables 4(d), 5(d) and 6(d) for the three groups, respectively. In the final steps relative significance Q_i, quantitative utility U_i and final complete ranking of each group are determined using Equations 12 and 13 and are summarized in table 4(e), 5 (e) and 6(e) for Group A, B and C, respectively.

Table 4 for Group 'A' shows the sequence as A4>A1>A2>A5>A3. It means that the best design alternative among these five configurations is A4 and the least preferable is A3. The same is shown in Table 4(e). This configuration will be further compared between the top design alternatives of each group.

The result of COPRAS method is obtained as B1>B4>B2>B5>B3 for Group 'B' configurations. In this group the best choice is B1 while the worst choice is B3. The best design concept of this group will also be compared with others group's best choices in the final stage of decision making method.

From Table 6(e), it is evident that the best concept is C5 while the worst is C2 and the ranking is as; C5>C4>C1>C3>C2. The best design alternative of this group will also be compared among the top members of the three groups so that the final optimum/best choice can be selected. Furthermore, it is clear from the calculations that the worst choices of each group are A3, B3 and C2.

Finally, COPRAS method is used to find out the best possible design concept among the top members of each group which are A4, B1 and C5. It is clear from Table 7(b) that the best choice is C5 among all the groups. This design concept can be further optimized by using available optimization techniques by conducting parametric studies.

Specimen	Crashworthiness Indicators		
	PCF (KN)	SEA (KJ/Kg)	CFE
A1	79.09	17.68	0.61
A2	92.65	19.18	0.57
A3	99.59	18.50	0.51
A4	81.58	19.34	0.69
A5	87.36	17.42	0.61

(a)

Specimen	Crashworthiness Indicators		
	PCF (KN)	SEA (KJ/Kg)	CFE
A1	0.180	0.192	0.205
A2	0.210	0.208	0.191
A3	0.226	0.201	0.170
A4	0.185	0.210	0.230
A5	0.198	0.189	0.204

(b)

Specimen	Crashworthiness Indicators		
	PCF (KN)	SEA (KJ/Kg)	CFE
A1	0.075	0.080	0.034
A2	0.088	0.087	0.032
A3	0.094	0.084	0.028
A4	0.077	0.088	0.038
A5	0.083	0.079	0.034

(c)

Specimen	S_{i+}	S_{i-}
A1	0.114	0.075
A2	0.119	0.088
A3	0.112	0.094
A4	0.126	0.077
A5	0.113	0.083

(d)

Specimen	Q_i	U_i	Rank
A1	0.206	95.821	2
A2	0.197	91.641	3
A3	0.185	86.079	5
A4	0.215	100.000	1
A5	0.196	91.211	4

(e)

Table 4: Group "A" tube system - COPRAS results (a) Decision Matrix (b) Normalized decision matrix (c) Weighted normalized decision matrix (d) Sum of the Weighted Normalized values of beneficial and non-beneficial attributes (e) Values of relative significance Q_i and quantitative utility U_i.

Specimen	Crashworthiness Indicators		
	PCF (KN)	SEA (KJ/Kg)	CFE
B1	103.71	22.95	0.72
B2	76.50	15.73	0.57
B3	85.96	15.84	0.57
B4	83.69	18.13	0.64
B5	93.79	17.22	0.61

(a)

Specimen	Crashworthiness Indicators		
	PCF (KN)	SEA (KJ/Kg)	CFE
B1	0.234	0.255	0.232
B2	0.172	0.175	0.182
B3	0.194	0.176	0.182
B4	0.189	0.202	0.207
B5	0.211	0.192	0.197

(b)

Specimen	Crashworthiness Indicators		
	PCF (KN)	SEA (KJ/Kg)	CFE
B1	0.097	0.107	0.039
B2	0.072	0.073	0.030
B3	0.081	0.073	0.030
B4	0.079	0.084	0.035
B5	0.088	0.080	0.033

(c)

Specimen	S_{i+}	S_{i-}
B1	0.145	0.097
B2	0.103	0.072
B3	0.104	0.081
B4	0.119	0.079
B5	0.113	0.088

(d)

Specimen	Q_i	U_i	Rank
B1	0.216	100.000	1
B2	0.199	92.233	3
B3	0.189	87.572	5
B4	0.206	95.515	2
B5	0.191	88.386	4

(e)

Table 5: Group "B" tube system - COPRAS results (a) Decision Matrix (b) Normalized decision matrix
(c) Weighted normalized decision matrix (d) Sum of the Weighted Normalized values of beneficial and
non-beneficial attributes (e) Values of relative significance Qi and quantitative utility Ui.

Specimen	Crashworthiness Indicators		
	PCF (KN)	SEA (KJ/Kg)	CFE
C1	76.23	17.78	0.60
C2	67.33	15.83	0.55
C3	70.42	16.34	0.58
C4	76.79	19.03	0.66
C5	69.82	21.51	0.75

(a)

Specimen	Crashworthiness Indicators		
	PCF (KN)	SEA (KJ/Kg)	CFE
C1	0.211	0.196	0.193
C2	0.187	0.175	0.174
C3	0.195	0.181	0.185
C4	0.213	0.210	0.210
C5	0.194	0.238	0.238

(b)

Specimen	Crashworthiness Indicators		
	PCF (KN)	SEA (KJ/Kg)	CFE
C1	0.088	0.082	0.032
C2	0.078	0.073	0.029
C3	0.081	0.075	0.031
C4	0.089	0.088	0.035
C5	0.081	0.099	0.040

(c)

Specimen	S_{i+}	S_{i-}
C1	0.114	0.0882
C2	0.102	0.0779
C3	0.106	0.0814
C4	0.123	0.0888
C5	0.139	0.0807

(d)

Specimen	Q_i	U_i	Rank
C1	0.193	85.736	3
C2	0.191	85.001	5
C3	0.191	85.097	4
C4	0.201	89.348	2
C5	0.225	100.000	1

(e)

Table 6: Group "C" tube system - COPRAS results (a) Decision Matrix (b) Normalized decision matrix (c) Weighted normalized decision matrix (d) Sum of the Weighted Normalized values of beneficial and non-beneficial attributes (e) Values of relative significance Qi and quantitative utility Ui.

Specimen	S_{i+}	S_{i-}
A4	0.180	0.133
B1	0.206	0.170
C5	0.198	0.114

(a)

Specimen	Q_i	U_i	Rank
A4	0.321	88.335	2
B1	0.317	87.209	3
C5	0.363	100.000	1

(b)

Table 7: Comparison among the best energy absorbers of each group (a) Sum of the weighted normalized values of beneficial and non-beneficial attributes (b) Values of relative significance Q_i and quantitative utility U_i.

6 CONCLUSIONS

A uni-sectional bi-tubular inner tubes arrangement is proposed which is placed inside a circular outer tube along with varying cross-sectional outer tubes. The configurations are axially crushed for energy absorption and crushing response. A decision making method known as COPRAS is employed to find out the optimal design alternative using the three conflicting criteria namely SEA, PCF and CFE. The study shows amazingly stable force-displacement curves for some of the proposed configurations along with competitive energy absorption indicators. The main findings of the study can be summarized as:

1. Bi-tube arrangement with uni-cross-section shows much more stable crushing than the conventional single or bi-tubular arrangement. Starting with a concertina, later converting to diamond modes, Group 'A' shows the most stable force-displacement curves while the Group 'B' shows some force variations about the mean load with relatively less stability than Group 'A'. The Group 'C', though showing less stability, shows better performance in other energy absorption parameters.

2. The proposed configurations show a comparative performance in energy absorption by utilizing proposed structural methodology, especially A4 configuration in Group 'A' with bi-circular inner tubes, B4 configuration in Group 'B' with pentagonal inner bi-tube arrangement and C5 configuration with hexagonal inner and outer tubes shows the high MCF, SEA, EA with relatively less PCF values. The highest specific energy absorption is seen in configuration B1 with a value of 23kJ/kg but the peak force is also at high levels. The C5 shows the SEA as 21.5kJ/kg but the PCF is 32.7% low in comparison to B1. The multi-corner configurations or the configuration having a direct contact with the outer tube forming a multi-cell with wall-supporting effect show better performance in energy absorption due to inertia and cell feature.

3. The highest ratio of mean crushing force to peak crushing force is observed in C5 configuration with 75% value while B1 configuration followed with a value of 72%. All other configuration shows values in fifties and sixties. Without any triggering mechanism, the values can be considered relatively high with better performance.

4. The best configuration among the different groups in terms of three conflicting criteria namely SEA, PCF and CFE is found to be the configuration C5 by using COPRAS. The weighting factors variation can change the decision. The A4 configuration is found as the second best followed by the B1 configuration. The B1 configuration shows a high PCF value which made the COPRAS to rank it as the third best configuration among the three groups.

The study shows some interesting results in the application and usage of inner bi-tubular arrangement with a single cross-section. The shape and placement has shown considerable effect on the energy absorption indicators. The placement in Group 'A' can give the stable crushing which can be helpful in automobile applications with reduced PCF values. In terms of SEA, the outer tube cross-section can also alter the results and can be optimized to perform a role with other optimized indicators.

Acknowledgement

References

ABAQUS, Version 6.15. "Abaqus analysis user's manuals." Simulia Dassault Systems, Rising Sun Mills, 166 Valley Street, Providence, RI 02909–2499, USA.

Abramowicz, W., and Jones, N., (1986). "Dynamic progressive buckling of circular and square tubes." Int. J. Impact Eng. 4(4): pp. 243–270.

Abramowicz, W., and Wierzbicki, T. (1989). "Axial crushing of multi corner sheet metal columns." J Appl Mech 56(1):113–20.

Ahmed, N., Xue, P., Kamran, M., Zafar, N., Mustafa, A., Zahran, M., S. (2017). "Investigation of the Energy Absorption Characteristics of Metallic Tubes with Curvy Stiffeners under Dynamic Axial Crushing." Latin American Journal of Solids and Structures, http://dx.doi.org/10.1590/1679-78253820.

Alexander, J.M., (1960). "An approximate analysis of the collapse of thin cylindrical shells under axial loading." Q. J. Mech. Appl. Math. (XIII): 10–15.

Alghamdi, A., Aljawi, A., and Abu Mansour, T., M. (2002). "Modes of axial collapse of unconstrained capped frusta." Int J Mech Sci 44:1145-61.

Aljawi, A., and Alghamdi, A. (2000). Inversion of frusta as impact energy absorbers, New York, USA: Pergamon; 511-19.

Chen, W., and Wierzbicki, T. (2001) "Relative merits of single-cell, multi-cell and foam-filled thin-walled structures in energy absorption." Thin- Walled Structures 39: 287-306.

Gang, Z., Suzhen, W., Guangyong S., Guangyao, Li, and Qing, Li. (2014). "Crushing analysis of foam-filled single and bi tubal polygonal thin-walled tubes." International Journal of Mechanical Sciences 87: 226–240.

Hosseini, M., Abbas, H., and Gupta, N., K. (2006). Straight fold analysis for axisymmetric crushing of thin walled frusta and tubes." Latin American Journal of Solids and Structures 3:345-360.

Hui, Z., and Xiong, Z. (2016). "Crashworthiness performance of conical tubes with nonlinear thickness distribution." Thin-Walled Structures 99: 35-44.

Jones, N. (2012). Structural impact, 2nd ed. Cambridge University Press.

Karagiozova, D., Alves, M., and Jones, N. (2000). "Inertia effects in axi-symmetrically deformed cylindrical shells under axial impact." International Journal of Impact Engineering 24:1083-115.

Karagiozova, D., and Alves, M. (2004). "Transition from progressive buckling to global bending of circular shells under axial impact—Part I: Experimental and numerical observations." Int. J. Solids Struct. 41:1565–1580.

Kashani, M., H., H. Alavijeh, S., Akbarshahi, H., and Shakeri, M. (2013). "Bi-tubular square tubes with different arrangements under quasi-static axial compression loading." Materials and Design 51:1095–1103.

Langseth, M., and Hopperstad, O., S. (1996). "Static and dynamic axial crushing of square thin walled aluminum extrusions." International Journal of Impact Engineering 18(7-8):949-68.

Langseth, M., Hoppers tad, O., S., and Bested, T. (1999). "Crashworthiness of aluminum extrusions: validation of numerical simulation, effect of mass ratio and impact velocity." International Journal of Impact Engineering 22:829–54.

Manmohan, D., G. (2015). "Deformation, energy absorption and crushing behavior of single, double and multi-wall foam filled square and circular tubes." Thin-Walled Structures. 90:1-11.

Marzdashti, E., S., Pirmohammad, S. and Marzdashti, S., E. (2016). "Crashworthiness analysis of s-shaped structures under axial impact loading." Latin American Journal of Solids and Structures http://dx.doi.org/10.1590/1679-78253430.

Pirmohammad, S. and Marzdashti, E., S. (2016). "Crushing behavior of new designed multi-cell members subjected to axial and oblique quasi-static loads." Thin-Walled Structures 108:291-304.

Qiu, N., Gao, y., Fang, J., Feng, Z., Sun, G. and Li, Q. (2015). "Crashworthiness analysis and design of multi-cell hexagonal columns under multiple loading cases." Finite Elements in Analysis and Design 104:89-101.

Seitzberger, M., Rammerstorfer, F., G., Degischer, H., P., and Gradinger, R., Blaimschein, M., and Walch, C. (2000). "Experimental studies on the quasi-static axial crushing of steel columns filled with aluminum foam," Int J Solids Struct. 37: 4125–47.

Sun, G., Y., Li, G., Y., Hou, S., J., Zhou, S., W., Li, W., and Li, Q. (2010). "Crashworthiness design for functionally graded foam-filled thin-walled structures." Mater Sci Eng. A. 527:1911–9.

Tang, Z., Shutian, L., Zhang, Z. (2013). "Analysis of energy absorption characteristics of cylindrical multi-cell columns." Thin-Walled Structures 62:75–84.

Tarlochan, F., Samer, F., Hamouda, A., M., S., Ramesh, S., and Karam, K. (2013). "Design of thin wall structures for energy absorption applications: Enhancement of crashworthiness due to axial and oblique impact forces." Thin-Walled Structures 71:7–17.

TrongNhan, T. (2017). "Crushing and theoretical analysis of multi-cell thin-walled triangular tubes under lateral loading." Thin-Walled Structures 115: 205–214.

Vinayagar, K., Kumar, S. (2017). "Crashworthiness analysis of double section bi-tubular thin-walled structures." Thin-Walled Structures 112:184–193.

Wierzbicki, T., and Abramowicz, W., (1983). "On the crushing mechanics of thin walled structures." J. Appl. Mech. Tran.50: pp. 727–739.

Xie, S., Weilin, Y., Ning, W., and Haihong, L. (2017). "Crashworthiness analysis of multi-cell square tubes under axial loads." International Journal of Mechanical Sciences 121: 106–118.

Xiong, Z., Hui Z., and Zhuzhu, W. (2015). "Axial crushing of tapered circular tubes with graded thickness." International JournalofMechanicalSciences 92:12–23.

Yafeng, C., Zhonghao, Bai., Linwei, Z., Yulong, W., Guangyong, S., and Libo, C. (2017). "Crashworthiness analysis of octagonal multi-cell tube with functionally graded thickness under multiple loading angles." Thin–Walled Structures 110: 133–139.

Yamashita, M., Gotoh, M. and Sawairi, Y. (2003). "Axial crush of hollow cylindrical structures with various polygonal cross-sections: numerical simulation and experiment." J. Mater. Process Technol. 140: 59–64.

Zahran, M., S., Xue, P., and Esa, M., S. (2016). "Novel approach for design of 3D-multi-cell thin-walled circular tube to improve the energy absorption characteristics under axial impact loading." International Journal of Crashworthiness.

Zahran, M., S., Xue, P., Esa, M., S., Abdelwahab, M., and Lu, G. (2016). "A New Configuration of Circular Stepped Tubes Reinforced with External Stiffeners to Improve Energy Absorption Characteristics Under Axial Impact." Latin American Journal of Solids and Structures http://dx.doi.org/10.1590/1679-78253231.

Zarei, H., and R., Kroger, M., (2008). "Optimization of the foam-filled aluminum tubes for crush box application." Thin-Walled Struct. 46: 214–21.

Zhang, Y., Sun, G., Y., Li., G., Y., Luo, Z., and Li, Q. (2012). "Optimization of foam-filled bi-tubal structures for crashworthiness criteria." Mater Des. 38: 99–109.

Zhang, X., Zhang, H. (2014). "Axial crushing of circular multi-cell columns." International Journal of Impact Engineering, 65: 110-125.